GEOPHYSICAL RESEARCH LETTERS, VOL. 20, NO. 2, PAGES 97-100, JANUARY 22, 1993

RAPID ESTIMATION OF RUPTURE DIRECTIVITY: APPLICATION TO THE 1992 LANDERS (M_S = 7.4) AND CAPE MENDOCINO (M_S = 7.2), CALIFORNIA EARTHQUAKES

Charles J. Ammon, Aaron A. Velasco, and Thorne Lay
The Institute of Tectonics and C. F. Richter Laboratory, University of California, Santa Cruz

Abstract. Using empirical Green functions with regional and teleseismic surface waves, it is possible to resolve fault finiteness effects, in many cases uniquely defining the fault plane for relatively large earthquakes. The technique requires very little data processing and can be applied in near-real time with the current distribution of seismic stations. The Landers strike-slip earthquake was dominated by two sub-events with predominantly north-northwestward rupture. The second sub-event was 1.5 times larger and rotated in strike by 12° counter-clockwise relative to the first. The Cape Mendocino thrust event had a relatively smooth rupture that propagated to the southwest on a shallow dipping fault.

Introduction

Near real-time information about large earthquakes is vital for the timely assessment of earthquake hazards associated with aftershocks, and estimation of potential hazards associated with stress changes on faults adjacent to the earthquake. The near real-time availability of seismic data from globally distributed seismic stations allows estimation of a point source moment tensor and the rupture duration within a few hours after the earthquake [Ekström, 1992]. However, existing techniques do not distinguish the fault plane from the auxiliary plane. We present a simple method to estimate first-order rupture finiteness information for relatively large earthquakes when an empirical Green function is available (a moderate-size precursory event or an aftershock with a similar fault orientation). Rupture directivity information can often remove the fault-plane ambiguity and help identify regions likely to have experienced the strongest ground acceleration. This latter information may help coordinate disaster response teams.

To isolate information on rupture directivity we deconvolve empirical Green functions [Hartzell, 1978] from the surface-wave recordings. Previous researchers have used empirical Green functions to estimate source parameters [e.g., Weidner and Aki, 1973; Patton, 1980; Hough et al., 1991]. We illustrate our procedure using two recent California earthquakes, the 1992 Cape Mendocino and Landers earthquakes (Figure 1, Table 1). We show that the rupture of the Landers event propagated to the northwest and contained two sub-events. The Cape Mendocino event ruptured smoothly to the southwest of the hypocenter in an up-dip direction. Source directivity identifies the fault plane in both cases.

Paper number 92GL03032
0094-8534/93/92GL-03032$03.00

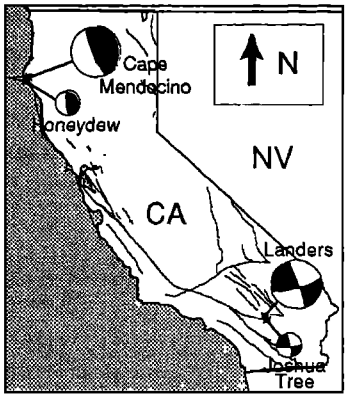

Fig. 1. Location and mechanisms of the Cape Mendocino, Honeydew, Landers, and Joshua Tree earthquakes. The EGF focal mechanism size is arbitrarily set to one-half that of the main shock.

Table 1. Source Parameters

Event	Date	Origin Time	M_S	Lat.	Lon.
Landers	6/28/92	11:57:35	7.4	34.200	116.500
Joshua Tree	4/23/92	04:50:22	6.1	34.100	116.400
Cape Mendocino	4/25/92	18:06:04	7.2	40.322	124.230
Honeydew	8/17/91	19:25:41	6.2	40.260	124.296

Source Time Function Isolation

Using the waveform from a small event as an empirical Green function (EGF) for source orientation, propagation, and instrument effects, we deconvolve the EGF from the mainshock waveform to estimate a relative source time function (RSTF). The true source time function can be estimated by correcting the RSTF for the EGF seismic moment and radiation effects.

The first step toward isolating the directivity effects is identification of the EGF. Ideally, the mainshock and the EGF should be collocated with identical mechanisms. Analysis of several large events with EGFs that are located within 100 km of the mainshock indicates stable RSTF recovery down to periods of about 10-20 s. In general, the larger the distance between the mainshock and the EGF, the lower the frequency for which the procedure is valid [Patton, 1980]. The size of the EGF influences the resolution of the time function. Moderate size events are optimal since they have adequate signal-to-noise ratios at longer periods. For large EGF's, EGF directivity may complicate the interpretation of the RSTFs. For the events utilized in this paper, these effects

are small for periods below 10 s, which is longer than the EGF corner period in each case.

The surface waves are extracted from the seismograms using group-velocity windows. The windows are referenced to the origin time and epicenter of each event, and the phase of the deconvolution is sensitive to these parameters. The mean of each seismogram is removed and the seismogram is tapered near the ends. The deconvolution is performed in the frequency domain using the water-level method [Helmberger and Wiggins, 1971]. Although not always the most effective deconvolution procedure [Sipkin and Lerner-Lam, 1992], water-level deconvolution is a reasonable choice when little information on noise is available. The bandwidth of our data is such that the water-level has little influence on the analysis.

Figure 2 illustrates the estimation of an RSTF for the Landers event. The EGF, from the Joshua Tree earthquake, is shown beneath the mainshock waveform and is scaled to ten

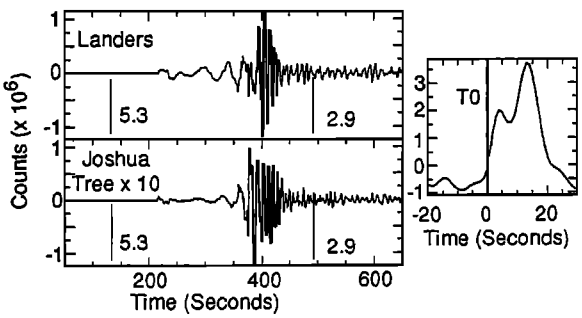

Fig. 2. The Love-Wave ground motion recorded at CCM, Cathedral Caves, Missouri due to the Landers and Joshua Tree earthquakes. The estimated RSTF obtained by deconvolving the Joshua Tree from the Landers ground motion. A zero-phase, low-pass, Butterworth filter with a corner at 10 seconds has been applied to the RSTF.

times its actual amplitude. The time of each seismogram is relative to each event's origin time and the vertical lines identify the Love-wave group-velocity window. To the right of the seismograms is the estimated RSTF with the vertical line labeled T0 identifying the zero phase time associated with the EGF. The deconvolution eliminates the common dispersion along the path, leaving only minor dispersive effects from within the main shock rupture dimensions.

The June 28, 1992 Landers, California Earthquake

The Landers earthquake occurred in the southern Mojave Block and ruptured a fault approximately 60-70 km in length. Early estimates of the focal mechanism [Ekström, Thio, personal communication, 1992] indicated that this event was a near-vertical strike-slip event on either a north-south or east-west striking fault. This earthquake was preceded by the April 23, 1992, M_L 6.1 near-vertical strike-slip Joshua Tree earthquake located approximately 30 km to the south. Directivity estimates for the April event indicate only a few seconds duration [Kanamori, personal communication, 1992]. The depth extent of rupture, delineated by aftershock distributions, is comparable for both events. Using the Joshua Tree waveforms as EGFs, we estimated 13 RSTFs using teleseismic and regional long-period stations obtained from the IRIS Gopher automatic dial-up system (Table 2).

The deconvolutions are stable with the exception of waveforms very close to nodes in the radiation patterns. The variation in the RSTFs is a strong function of azimuth (Figure 3). To the northeast/east and the southwest/west the RSTFs contain two distinct pulses labeled 1 and 2 in Figure 3. The overlap of these pulses at stations to the northwest (BKS and COL) indicates a roughly northward propagating rupture and identifies the north-south striking plane as the fault. Since the pulse separation varies from 0 to 9 s and the wave velocities involved are about 3.5 km/s, we can estimate that the two pulses are from regions of the fault about 31 km apart. Qualitative arguments are strong in this particular case, but more quantitative information can be obtained.

To locate the onset of the Landers earthquake and the two sub-events in the time function, we used directivity calculations on features in the RSTFs such as has been done for teleseismic P-waves [e.g., Schwartz and Ruff, 1985]. The analysis is based on the relationship, $\delta t = t_o - \Gamma\Delta$, where δt is the time difference between two features, t_0 is the time between the events, and Δ is the distance between the two events. The

Table 2. Station Locations

Station	Latitude (N°)	Longitude (W°)	Landers Δ(°)	Landers Az(°)	Cape Mendocino Δ(°)	Cape Mendocino Az(°)
ANMO	34.946	106.460	8.3	82.0	15.1	105.2
BKS	37.877	122.240	5.9	309.9	-	-
CCM	38.056	91.245	20.7	72.0	25.6	84.3
COL	64.900	147.790	36.1	337.9	-	-
GUMO	13.588	-144.870	89.5	286.0	-	-
HRV	42.507	71.562	35.9	63.1	39.0	69.0
KIP	21.423	158.010	38.6	261.8	34.3	246.9
KONO	59.649	-9.598	76.5	25.0	73.4	22.5
MAJO	36.543	-138.210			72.5	303.2
NWAO	-32.927	117.230	135.7	255.9	-	-
PAS	34.148	118.120	-	-	7.8	140.0
SNZO	-41.310	-174.700	98.2	225.2	-	-
TOL	39.881	4.045	-	-	83.3	42.0

directivity parameter, Γ, is given by $\Gamma \equiv \cos\theta/c$ where θ is the azimuth of the station relative to the azimuth of a line connecting the events, and c is the surface-wave phase velocity. Since the RSTFs contain signal with periods between 200 s and 10 s period, no single phase velocity is appropriate. We use the average phase-velocity associated with the Love (4.38 km/s) or Rayleigh (3.85 km/s) Airy phase arrivals since most of the energy in the teleseismic signals is concentrated in those packets. The constant phase-velocity approximation causes only about 15% uncertainty in subsequent offsets and has no effect on rupture azimuth. To estimate Δ and t_0, the linear model is investigated systematically for each azimuth. The preferred azimuth corresponds to the direction producing the best linear correlation coefficient. In Figure 4 (Left), we present the directivity results for the second sub-event relative to the onset of the motion of the Landers earthquake. The inset

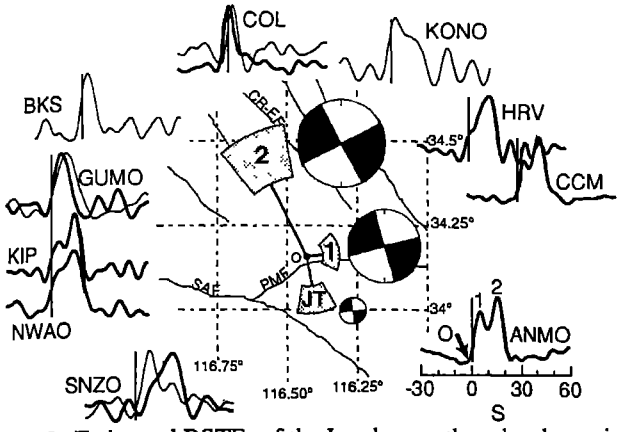

Fig. 3. Estimated RSTFs of the Landers earthquake shown in azimuthal distribution (ANMO excepted). Thick lines are estimates obtained from Love waves, thin lines from Rayleigh waves. The time between the onset of the RSTF and the vertical line represents the phase shift between the main shock and the EGF due to errors in origin time or location. In the center are the results of the directivity analysis for the location of the two Landers sub-events and the Joshua Tree earthquake relative to the onset of motion of the Landers event. Shaded regions identify the formal errors for the relative locations. Estimated mechanisms of the two sub-events are also shown. SAF San Andreas Fault, CR-EF Camp Rock Emerson Fault, PMF Pinto Mountain Fault, JT Joshua Tree earthquake.

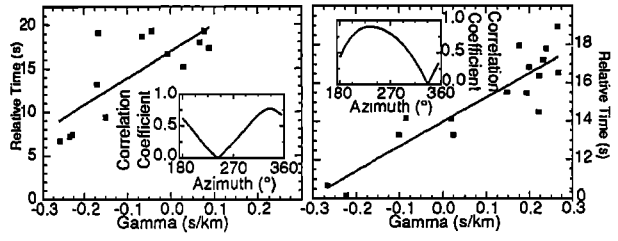

Fig. 4. (Left) Directivity analysis of the second sub-event relative to the onset of motion of the Landers earthquake. The inset shows the variation of the linear correlation coefficient as a function of azimuth from the onset to the center of the second sub-event. The maximum value occurs at a strike of 335° and the corresponding fit is shown. Squares correspond to observations, the best fitting line is also shown. (Right) Directivity analysis of the Cape Mendocino, format is the same.

contains the variation of the linear correlation coefficient as a function of the azimuth and indicates that the best correlation occurs for an azimuth of 335°. The least-squares, straight line corresponding to this azimuth is shown and individual observations are presented as squares. Similar analyses are made for other features in the source functions. Numerical details for all the directivity calculations are contained in Table 3.

The Landers event ruptured from just north of the Joshua Tree event, toward the north-northwest. The relative locations of the onset, the sub-events, and the Joshua Tree EGF are presented in the center of Figure 3. The formal directivity measurements suggest that the first pulse is located slightly east of the epicenter. However, this location is not reliably resolved due to complexity in the higher frequency component

Table 3. Directivity Analysis

Event Pair	Time Separation (s)	Correlation Coefficient	Distance (km)	Azimuth (°)
	Landers			
Onset to EGF	2.3±0.6	0.70	12.5±3.9	170±20
Onset to S1	7.7±0.4	0.66	7.0±2.4	80±35
Onset to S2	16.9±1.1	0.77	30.7±7.6	335±15
Onset to End	26.8±1.5	0.60	25.3±10.2	350±20
S1 to S2	9.5±1.1	0.83	34.2±7.0	330±20
	Cape Mendocino			
Onset to EGF	-3.9±0.3	0.89	11.1±1.6	130±25
Onset to Peak	6.9±0.2	0.85	6.6±1.1	230±30
Onset to End	14.0±0.3	0.90	12.7±1.6	235±25

of the first pulse. The unambiguously resolved feature is that the second pulse lies to the north-northwest. Relative to the onset, a rupture velocity of about 2 km/s is inferred, but relative to the first pulse a higher rupture velocity of 3.6 km/s is found. This discrepancy is in part caused by bias of onset times due to the effects of noise and band-pass filtering, and in part by uncertainty in the timing of the first peak. The rupture velocity uncertainty does not affect the rupture azimuth or distance estimates.

Systematic differences in the relative sub-event amplitudes between traces deconvolved from Rayleigh and Love waves (Figure 3) suggest a mechanism change during rupture. These patterns can be used to determine the sub-event mechanisms relative to the EGF. We assume vertical strike-slip faulting for the EGF and the sub-events to reduce the azimuthal dependence of the surface-wave radiation patterns to simple sin(2θ) and cos(2θ) terms and omit stations strongly influenced by directivity such as COL and BKS. We measured the relative sub-event amplitudes by assuming simple Gaussian shapes for each sub-event and modeling the RSTFs. To estimate the relative moment and the strike for the j^{th} sub-event, we invert for the amplitude and strike using

$$F_{ij} = A_j \sin[2(\theta_i - \theta_j)]/\sin[2(\theta_i - \theta_o)] \qquad (1)$$

F_{ij} is the amplitude of the sub-event at the i^{th} station, A_j is the amplitude of the sub-event relative to the EGF, θ_i is the station azimuth (with an adjustment for Love waves, $\theta_i = \theta_i + \pi/4$), θ_j is the sub-event fault strike, θ_o is the strike of the EGF. The nonlinear inversion was performed by iteratively solving linearized versions of (1).

The fits of this model to the sub-event amplitudes are good and the formal errors from the linearized inversion are small (Figure 5). The curves show the predicted amplitude ratios of the surface waves for the sub-event relative to the EGF, and the squares are the measured amplitude ratios. The estimated moment ratio of the second sub-event to the first sub-event is approximately 1.5. The strike changes from the assumed 353° for the Joshua Tree earthquake to 344° for sub-event 1 and then to 332° for sub-event 2. These values are consistent with the variation in the strike of the surface rupture [K. Sieh, R. S. Anderson, personal communications, 1992] and are consistent with the rupture directions determined in the directivity analyses.

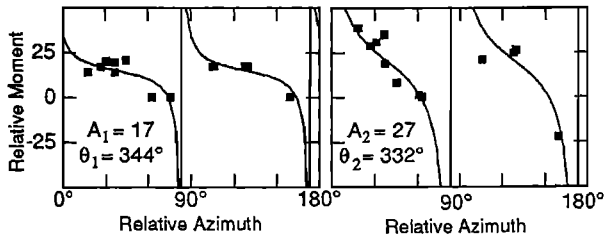

Fig. 5. Amplitude modeling of the Landers sub-events relative to the Joshua Tree mechanism. (Left) Sub-event 1 (Right) Sub-event 2. The squares identify observations, the curves are the best-fitting least-squares model. Also listed are the relative moment and strike of the best fitting mechanisms.

The April 25, 1992 Cape Mendocino Earthquake

On April 25, 1992 an M_S = 7.2 earthquake occurred in northern California, near the Mendocino Triple Junction. The preliminary thrust mechanism is very similar to the August 17, 1991 Honeydew (M_S = 6.2) event, located approximately 20 km south of the Cape Mendocino epicenter. However, it was not immediately known whether a low angle or a steeply dipping fault ruptured in the April event.

To estimate the rupture parameters we used the Honeydew event as an EGF and performed a deconvolution similar to that described above. The RSTFs associated with this event are simpler than the Landers earthquake but variations in rise-time and pulse width are detectable (Figure 6). Directivity modeling (Figure 4, Right) for this event suggests that the rupture propagated southwestward, which would correspond to updip on a shallow dipping fault (Figure 1). We find the Cape

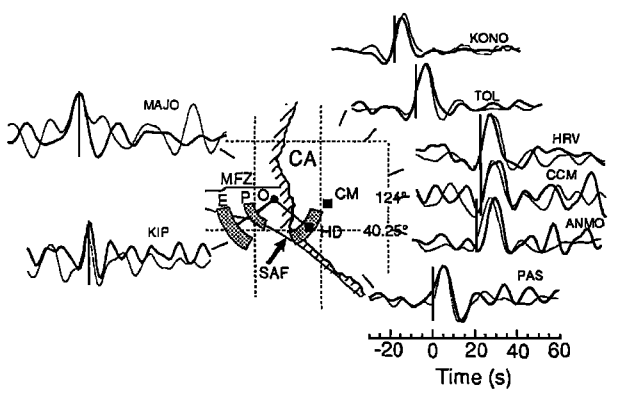

Fig. 6. Cape Mendocino earthquake RSTFs. In the center are the relative locations of the peak (P) and end (E) times, and the Honeydew earthquake (HD) relative to the onset of motion (O) of the Cape Mendocino event. The shaded regions illustrate the formal uncertainties in the relative locations. The hatched line is the coast of northern California. CM is the CALNET location of Cape Mendocino event. MFZ identifies the Mendocino Fracture Zone, SAF identifies the San Andreas Fault, and the grid spacing is 0.25°.

Mendocino event initiated at an azimuth of 310° and a distance of 11 km from the Honeydew earthquake. This azimuth coincides with the strike of the EGF (311°), suggesting that these earthquakes may have ruptured the same fault.

Discussion

The analysis of directivity using surface waves is comparable to previous studies using body waves. However, the range in the directivity parameter Γ is much larger for surface waves. In fact, surface waves provide the maximum far-field directivity information since their phase velocities approach the limit of the earth's elastic velocities. We have also performed body-wave deconvolutions for each of these earthquakes. For the Landers event, the P-wave deconvolutions were complicated due to a sensitivity to the nodal planes of a vertical strike-slip fault or simply noise in the EGF P waveforms. Deconvolution of the Landers SH waves results are consistent with the surface-wave results. For the Cape Mendocino event, P waves deconvolutions were stable and contained higher frequencies than the surface-waves RSTFs. Combining body and surface wave RSTFs will provide the best constraints on the time history of faulting.

Acknowledgments. We thank researchers at the California Institute of Technology and Harvard for providing rapid information about these earthquakes. We also thank S. Schwartz for providing the directivity program and reviewing the manuscript and two reviewers for their suggestions. This work was supported by NSF Grant EAR-9017767, a grant from the southern California Earthquake Center, and the W. M. Keck Foundation. Contribution number 179 of the Institute of Tectonics and C. F. Richter Seismological Laboratory.

References

Ekström, G., Quick CMTs - What's the next step?, 4th Annual IRIS Workshop, April, Sante Fe, NM, 1992.

Hartzell, S., Earthquake aftershocks as Green's functions, Geophys. Res. Letters, 5, 1-5, 1978.

Helmberger, D., and R. A. Wiggins, Upper mantle structure of the mid-western United States, J. Geophys. Res., 76, 3229-3245, 1971.

Hough, S. E., L. Seeber, A. Lerner-Lam and J. G. Armbruster, Empirical Green's function analysis of Loma Prieta aftershocks, Bull. Seismol. Soc. Am., 81, 1737-1753, 1991.

Patton, H., Reference point equalization method for determining the source and path effects of surface waves, J. Geophys. Res., 85, 821-848, 1980.

Schwartz, S. Y., and L. J. Ruff, The 1968 Tokachi-Oki and the 1969 Kurile Islands earthquakes: Variability in the rupture process, J. Geophys. Res., 90, 8613-8626, 1985.

Sipkin, S. A., and A. L. Lerner-Lam, Pulse-shape distortion introduced by broadband deconvolution, Bull. Seismol. Soc. Am., 82, 238-258, 1992.

Weidner, D. J., and K. Aki, Focal depths of mid-ocean ridge earthquakes, J. Geophys. Res., 78, 1818-1831, 1973.

C. Ammon, T. Lay, A. Velasco, Institute of Tectonics, Applied Sciences Bldg., University of California, Santa Cruz, CA 95064.

(Received July 22, 1992;
revised October 6, 1992;
accepted November 3, 1992.)